Carbon Clusters Hot Paper

DOI: 10.1002/ange.201406570

The Structure and Stability of Magic Carbon Clusters Observed in Graphene Chemical Vapor Deposition Growth on Ru(0001) and Rh(111) Surfaces**

*Junfeng Gao and Feng Ding**

Abstract: *To improve the atomically controlled growth of graphene by chemical vapor deposition (CVD), understanding the evolution from various carbon species to a graphene nucleus on various catalyst surfaces is essential. Experimentally, an ultrastable carbon cluster on Ru(0001) and Rh(111) surfaces was observed, while its structure and formation process were still under debate. Using ab initio calculations and kinetic analyses, we disclose a specific type of carbon cluster, composed of a C_{21} core and a few dangling C atoms, which is exceptional stable in a size range from 21 to 27 C atoms. The most stable one of them, an isomer of C_{24} characterized by three dangling C atoms attached to the C_{21} core (denoted as C_{21}-3C), is the most promising candidate of the experimental observation. The ultrastability of C_{21}-3C originates from both the stable core and the appropriate passivation of the dangling carbon atoms by the catalyst surface.*

Graphene was broadly studied for many applications, such as ultrafast transistors[1,2] or transparent and flexible electrodes,[3,4] because of the recorded electron/hole mobility,[5] extremely high thermal conductivity,[6,7] and superior mechanical performance.[8,9]

Among the known methods of graphene synthesis, chemical vapor deposition (CVD) is the best way to achieve high-quality single- or few-layer-thick graphene with a macroscopic area (up to 10000 cm^2) at a reasonable price, and therefore it was extensively explored both experimentally and theoretically.[10–28] In a CVD experiment, the transition-metal surface, on which graphene is formed by self-assembly of dissociated or deposited C atoms or radicals, plays a crucial rule. To date, a cornucopia of transition metals, such as Ru,[11,29] Rh,[30] Ir,[11] Cu,[17,21] Ni,[31] Pt,[23] Au,[32] and their metal alloys (i.e. Ni/Mo[19] and Ni/Cu[20]) were proved to be suitable for CVD of graphene.

The first stage in the growth of graphene by CVD —the nucleation of graphene on the catalyst surface—determines both the density of the nuclei and the concentration of the grain boundaries in the final product. Therefore, the nucleation of graphene has been intensively studied recently.[10–18] Theoretically, the evolution of C clusters and the size-dependent C formations on the catalyst surface have been investigated to determine the nucleation barrier and size of the nuclei under various growth conditions.[13] Previous theoretical explorations have shown that, by carefully optimizing the experimental conditions, the size of the nuclei can be controlled between $N = 20$–100 C atoms.[13–15] Therefore the structures and stabilities of the carbon clusters in this range are crucial for understanding the nucleation of graphene.

For the nucleation of graphene on Ru(0001) and Rh(111) surfaces, an astonishing experimental observation is the existence of ultrastable carbon clusters of about 1 nm in diameter.[33–35] Although different feedstock (e.g., C_2H_4,[33,34] $C_{12}H_{24}$,[33] and C_{60}[35]) were used in the graphene synthesis, nearly all the decomposed C atoms on the catalyst terrace were observed in the form of an uniform ultrastable cluster in a temperature range of 870–1000 K, indicating that this cluster is superior to others in a large size range. Mimicking the terminology of cluster science, we hereafter call it "magic cluster".

However, because of the high curvature at the edges of the cluster and the influence of the metal surface, scanning tunneling microscopy (STM) was unable to reveal the precise atomic structure of the magic cluster. As its size is close to that of a coronene molecule ($C_{24}H_{12}$), the magic carbon cluster was once suspected to be the dehydrogenated coronene, that is, the C_{24} with seven six-membered rings, namely 7-6MRs[36] or 7-C6.[33,34] Latterly, by systemically searching the sp^2 hybridized C clusters on various metal surfaces, we suggested that a closed core–shell isomer of C_{21}, which was characterized as one hexagon surrounded by three hexagons and three pentagons alternatively, was much more stable than the 7-6MRs. Therefore, the C_{21} isomer was considered as the observed magic cluster.[36]

In this manuscript, using density functional theory (DFT) calculations we present a new ultrastable isomer of C_{24}, which has the core of the aforementioned C_{21} and three dangling C atoms attached to the three pentagons (denoted as C_{21}-3C).

[*] Dr. J. Gao, Prof. F. Ding
Beijing Computational Science Research Center
Beijing, 100084 (China)
E-mail: feng.ding@polyu.edu.hk
Homepage: http://myweb.polyu.edu.hk/~tcfding/
Dr. J. Gao, Prof. F. Ding
Institute of Textiles and Clothing
Hong Kong Polytechnic University, Hong Kong (China)

[**] We thank Prof. Zhenyang Lin of HKUST for useful discussion. Support by National Natural Science Foundation of China (grant numbers 11304008 and 21273189) and Hong Kong GRF grants (grant numbers B-Q35N and B-Q26K), Development Fund of China Academy of Engineering Physics (grant number 2013B0302056) and China Postdoctoral Science Foundation (grant numers 2014T70030 and 2013M530019) are acknowledged. All the calculations were performed on TianHe-1(A) of National Supercomputer Center in Tianjin.

Supporting information for this article is available on the WWW under http://dx.doi.org/10.1002/anie.201406570.

The C_{21}-3C, with a much lower formation energy than the C_{21} and 7-6MRs, corresponds to the global energetic minimum and dominates the population in a large cluster size range, $20 \le N \le 30$ C atoms on Ru(0001) and Rh(111) surfaces. This study proposes a more probable candidate for the experimentally observed magic cluster during the growth of graphene by CVD and explains its significant stability on both Ru(0001) and Rh(111) surfaces.

To demonstrate the stability and formation of the C_{21}-3C isomer, we proposed an isomerization from 7-6MRs to C_{21}-3C on the Ru(0001) surface. Details of the DFT calculations are found in the Supporting Information in section S2. Figure 1a

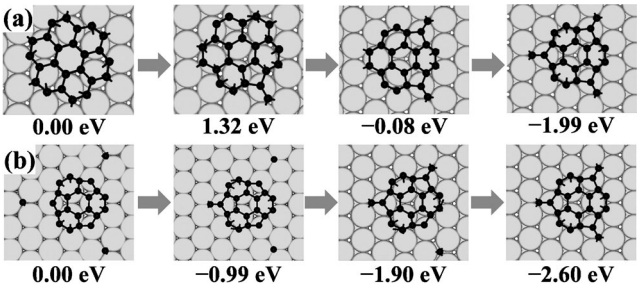

Figure 1. a) Isomerization from 7-6MR to C_{21}-3C of the C_{24} carbon cluster on the Ru(0001) surface. b) A core–shell C_{21} adsorbs three carbon adatoms and becomes the C_{21}-3C isomer on the Ru(0001) surface.

shows the transformation from 7-6MRs to C_{21}-3C by successive rearrangement of the three edge C–C bonds. The first bond rotation leads to a metastable structure with a 1.32 eV increase in energy. After that, the second bond rotation is −0.08 eV lower in energy than 7-6MRs, implying that this structure is thermodynamically more stable than 7-6MRs. With the third bond rotation, the energy of the final C_{21}-3C cluster is greatly reduced to −1.99 eV eventually. Such a remarkable energy reduction implies that the C_{21}-3C isomer is much more stable than the initial 7-6MRs. With this information at hand, the population ratio of 7-6MRs to C_{21}-3C. The population ratio of them in the thermal equilibrium can be estimated by Equation (1)

$$P_{7\text{-}6MR}/P_{C21\text{-}3C} = \exp(-1.99\,\text{eV}/k_B\,T) = 10^{-11} \quad (1)$$

at the experimental temperature of 900 K, where k_B is the Boltzmann constant and T is the temperature. Besides, isomerization from 7-6MRs to C_{21}-3C should easily occur at the experimental temperature of about 900 K as the energy barrier for a C–C bond rotation is only 1.38 eV (see Figure S3a), which is slightly lower than the bond rotation of the graphene zigzag edge on the Co surface.[22] These results imply that the observation of 7-6MRs after dehydrogenation of coronene on the Ru(0001) surface is nearly impossible.[33]

Let us consider the stability of the C_{21}-3C relative to the previous proposed C_{21} cluster on the Ru(0001) surface.[36] The C_{21}-3C cluster can be formed by a C_{21} cluster adsorbing three more C atoms from the catalyst surface (Figure 1b). The barrier of these three atomic adsorption processes are extremely low, less than 1.0 eV (see Figure S3b), and energy reductions are −0.99, −1.90, and −2.6 eV, respectively. Considering that the formation energy of a C monomer on the catalyst surface is about 0.55 eV higher than that of graphene, the formation energy of C_{21}-3C is about 1.0 eV lower than that of the core–shell C_{21} cluster, the most stable cluster shown in a previous study.[36] Thereby, if there are sufficient C monomers on the catalyst surface, up to $[1-\exp(-2.6\,\text{eV}/k_B\,T)] \approx 99.99\,\%$ of the core-shelled C_{21} clusters will be quickly transformed into the branched C_{21}-3C isomer in a temperature range of 870–1000 K.

This analysis clearly shows that the branched C_{21}-3C is energetically superior to the dehydrogenated 7-6MRs and the core–shell C_{21} cluster. To understand the ultrastability of C_{21}-3C on the catalyst surface, let us examine its structural and electronic properties.

Both C_{21} and C_{21}-3C have nine active edge atoms. There is one dangling bond at each edge atom of the hexagon and two dangling bonds at each edge atom of the pentagon (for C_{21}) or the dangling carbon atom (for C_{21}-3C), thereby both C_{21} and C_{21}-3C have 12 dangling bonds (see Figure 2a,d). However,

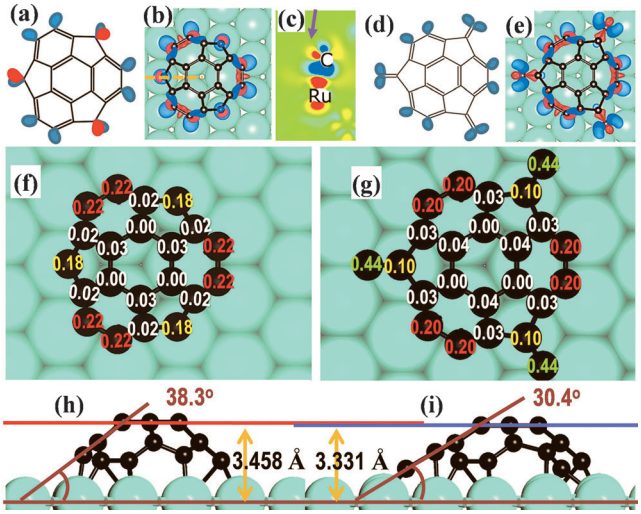

Figure 2. The schematics of dangling bonds of a) C_{21} and d) C_{21}-3C. Top view of the differential charge densities of b) C_{21} and e) C_{21}-3C on the Ru(0001) surface. c) Cross-section view of the differential charge densities of C_{21}@Ru(0001). The arrow points to the unpassivated dangling bond of the edge C atom. Bader charge analyses (in |e|) of f) C_{21} and g) C_{21}-3C on the Ru(0001) surface. h–i) The optimized C_{21} and C_{21}-3C structures on the Ru(0001) surface.

the arrangement of paired dangling bonds on the edge of the pentagon of C_{21} is different from that on the dangling C atom of C_{21}-3C. On the edge of a pentagon, the C atom tends to be sp^3 hybridized and the four σ bonds tend to be tetrahedrally distributed in space. As a consequence, one dangling bond on the edge of a pentagon of C_{21} flips upwards and thus was not efficiently passivated by the metal surface as evidenced by the differential charge densities near the edge atom (the red dangling bonds of Figure 2b,c and Figure S4). As only one dangling bond can be passivated by the metal surface, the edge C atom of the pentagon locates on top of a metal atom.

Different from C_{21}, the dangling atom of C_{21}-3C is sp^2 hybridized with one double bond and two dangling bonds according to the analysis of differential charge densities (Figure 2e). The arrangement of the two dangling bonds tends to be in the same plane of the tilted pentagon as the characteristic of the sp^2 C network (see Figure 2d). As a consequence, all edge-dangling bonds can be effectively passivated by the metal surface. To passivate both dangling bonds effectively, all the three dangling atoms of the C_{21}-3C locate near hollow and bridge sites of the metal surface as can be clearly seen in Figure 2e,i and Figure S4. The length of the outermost C–C bond of C_{21}-3C is about 1.44 Å.

The above-mentioned analyses explicitly explain the high stability of C_{21}-3C relative to C_{21} stems from the more effective passivation of the dangling atoms on the catalyst surface. As calculated in a previous study,[36] the binding energies of C_{21} on Ru(0001), Rh(111), Ir(111) surfaces were 16.9, 18.1, and 17.6 eV, respectively, which are significantly larger than the binding energies of core–shell C_{20} and 7-6MRs. Analyses using the same method showed that the binding energies of C_{21}-3C were further increased to 22.5, 23.1, and 21.9 eV on these metal surfaces, respectively, which were 5.6, 7.0, and 4.3 eV higher than those of C_{21} (Table S6), although both configurations possess the same number of active edge atoms. The large binding energies further validated the efficient passivation of the three dangling atoms of C_{21}-3C.

The stronger binding between C_{21}-3C and the catalyst surface relative to that of C_{21} is also verified by the Bader charge-transfer analysis. As shown in Figure 2f,g, the total charge transfer from the metal to C_{21} is about 2 |e|, which is much smaller than that from the metal to C_{21}-3C, about 3 |e|. The difference originates from the edges of the pentagons, where the charge transferred to an edge atom of a pentagon of C_{21} is about 0.18 |e| while the charge transferred to a dangling C atom of C21-3C is about 0.44 |e|.

The height of the experimentally observed magic carbon cluster is about 1 Å higher than that of coronene on the catalyst surface.[34] As shown in Figure 2 h,i and Table S5, the height of C_{21}-3C is close to that of C_{21}, which was proved to be about 1.23 Å higher than coronene.[36] That is, C_{21}-3C is about 1.0–1.1 Å higher than coronene on the catalyst surface, which agrees well with the experimental observations.[34]

Now, let us consider the stability of C_{21}-3C on a metal surface from the viewpoint of aromaticity. There are two typical nonplanar π-conjugated polycyclic aromatic hydrocarbon (PAH) molecules of a similar size, $C_{20}H_{10}$ (corannulene, synthesized in 1991[37]) and $C_{21}H_{12}$ (sumanene, synthesized in 2003[38]), and both were extensively studied before.[39–43] As the C_{5v} symmetry of C_{20} is different from that of the Ru(0001) surface, C_{20} on the Ru(0001) surface is less stable than C_{21}. In comparison with C_{21}, C_{21}-3C on Ru(0001) has a similar bonding situation as sumanene (see Figure S6 and Table S6 for a detailed discussion). They both show similar bond angels in the pentagon (about 103°) and the bond length difference in the hexagons of C_{21}-3C on Ru(0001) is only 0.014 Å, which is even smaller than that of sumanene (0.046 Å).[44] This implies that C_{21}-3C on a metal surface can be viewed as a typical nonplanar π-conjugated aromatic C cluster.[42,44] In contrast, C_{21} on a Ru surface has much larger bong angles in its pentagon (about 107°) and bond length difference in its hexagons. C_{21}-3C can be viewed as a derivative of the extended π-conjugated sumanene shown in Figure S6e and Ref. [45].

Moreover, the simulated STM images of the C_{21}-3C cluster on Ru(0001) are also in good agreement with its experimental images (see Figure S7).[33,35] The simulated STM images of C_{21} also correspond well to the experimental images.[36] This is attributed to the invisibility of the three dangling atoms because of their lower positions on the metal surface (Figure 2i). Similarly, the STM images of C_{21} and C_{21}-3C on Rh(111) and Ir(111) surfaces (Figure S8) are close to each other as well.[34]

With these compelling evidences and analyses, C_{21}-3C is expected to be the observed magic graphene cluster grown by CVD. As shown in a previous study, C_{21} has a stability similar to that of the 7-6MR isomer on Ru(0001) and Rh(111) surfaces, and thus it corresponds to a local minimum in the size range of $N < 24$ C atoms.[36] How stable is C_{21}-3C relative to C_{21} and other clusters? As shown in Figure 3, another two carbon clusters with one and two dangling edge atoms, namely C_{21}-1C (Figure 3b) and C_{21}-2C, respectively (Figure 3d), are also very stable. To fully address the stability of C_{21}-3C and its role in graphene nucleation, we systematically explored two serious of C clusters, i) those composed of pentagons and hexagons only as studied previously[13,14,18,36] and ii) those with one or a few dangling C atoms attached to the pentagons of the C_{21} core, on three catalyst surfaces: Ru(0001), Rh(111), and Ir(111). The most stable structures and corresponding formation energies of the clusters on Ru(0001), Rh(111), and Ir(111) surfaces were shown in Figure 3g, S9, S10 and S11, respectively. To find the lowest-energy structures in this regime, many different isomers were also considered (for example, some explored structures of C_{24}, C_{28}, C_{29} and C_{30} are shown in Figure S12).

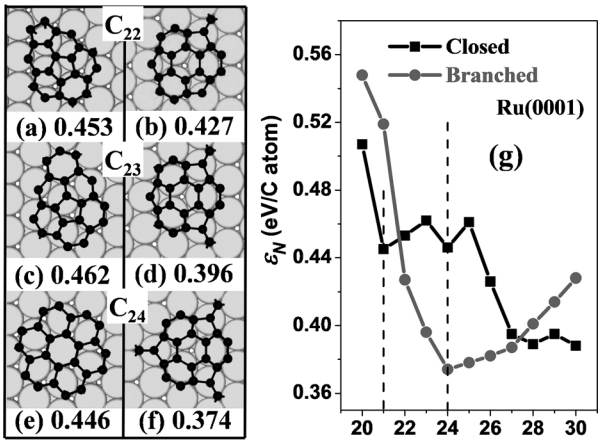

Figure 3. The most stable core–shell sp^2 network and branched C_N ($N = 22, 23, 24$) clusters on Ru(0001) surface (left panel) and the formation energies ε_N (in eV per C atom) of the most stable C_N ($N = 20$–30) clusters of each type on the Ru(0001) surface.

For C_N on all the three catalyst surfaces, in the explored cluster size region ($20 \le N \le 30$), the C_{21}-3C represents

a global energetic minimum (see Figure 3g). On a Ru-(0001) surface, the formation energy per C atom of the C cluster keeps dropping from $N=20$ to $N=24$ and then keeps rising from $N=24$ to $N=30$. This characteristic makes C_{21}-3C a deep global energetic minimum in the size range of $20 \le N \le 30$. Although C_{21} and 7-6MRs also correspond to two local minima in the energy curve of the core–shell clusters (vertical dash lines in Figure 3g),[36] their formation energies are much higher than that of the branched C clusters on Ru(0001). This means that the branched C clusters possess the highest stability in the vicinity of $N=24$ C atoms on Ru(0001) surface. It is important to note that the C clusters on both Rh(111) and Ir(111) surfaces exhibit characteristics similar to those on Ru(0001) (Figures S9–11), implying that the above analyses may be universal for graphene CVD growth on metal surfaces.

To quantify the population of the C_{21}-3C cluster on metal surface under different growth condition, let us introduce the chemical potential difference between the C atom in feedstock and in graphene on the catalyst surface, $\Delta\mu$. According to the classical theory of crystal nucleation,[46] the population of a cluster can be estimated by Equation (2),

$$P_N = \exp(-\Delta G/kT), \quad (2)$$

where $\Delta G = E_N - N\times\Delta\mu$ is the Gibbs free-energy and $E_N = N\times\varepsilon_N$ is the total formation energy of a cluster C_N. The calculated ΔG and normalized fraction P_N in the size range of $20 \le N \le 30$ with $\Delta\mu = 0.0$, 0.1, 0.2, and 0.3 eV are shown in Figure 4, respectively. The kinetic stability of the clusters on the three catalyst surfaces is presented as follows:

1) On the Ru(0001) surface, the Gibbs free-energy of the C_{21}-3C cluster is a deep local minimum for a large range of $\Delta\mu$ (Figure 4a). Because of the exceptional stability, the population of C_{21}-3C is always dominant in the explored size range (> 89%; Figure 4b).

2) On the Rh(111) surface, C_{21} has a lower formation energy than that of C_{21}-3C at $\Delta\mu = 0.0$ eV. But when $\Delta\mu$ becomes slightly larger, that is, $\Delta\mu > 0.2$ eV (common condition), C_{21}-3C becomes more stable than C_{21} (Figure 4c). Thus C_{21}-3C is the dominating species and can only be observed in the range of $\Delta\mu \ge 0.2$ eV (Figure 4d).

3) On the Ir(111) surface, the small clusters, C_{21}, branched C_{22} and C_{23} are more stable than C_{21}-3C in the range of $\Delta\mu <$ 0.2 eV (Figure 4e). The dominating clusters is C_{21} at $\Delta\mu =$ 0.0 eV but there is no dominating cluster from $\Delta\mu =$ 0.1 to 0.3 eV (Figure 4f).

These analyses indicate that the probability for observing the magic cluster on the three metal surfaces follows the order of Ru(0001) > Rh(111) > Ir(111). Such a trend is in perfect agreement with the known experimental facts. Experimentally, most reported magic clusters were observed on Ru-(0001)[33,35] and a few on Rh(111).[35] Although Ir(111) has a catalyst surface similar to Rh(111) and Ru(0001) for graphene growth, no uniformed C clusters were obsevered on it.[47]

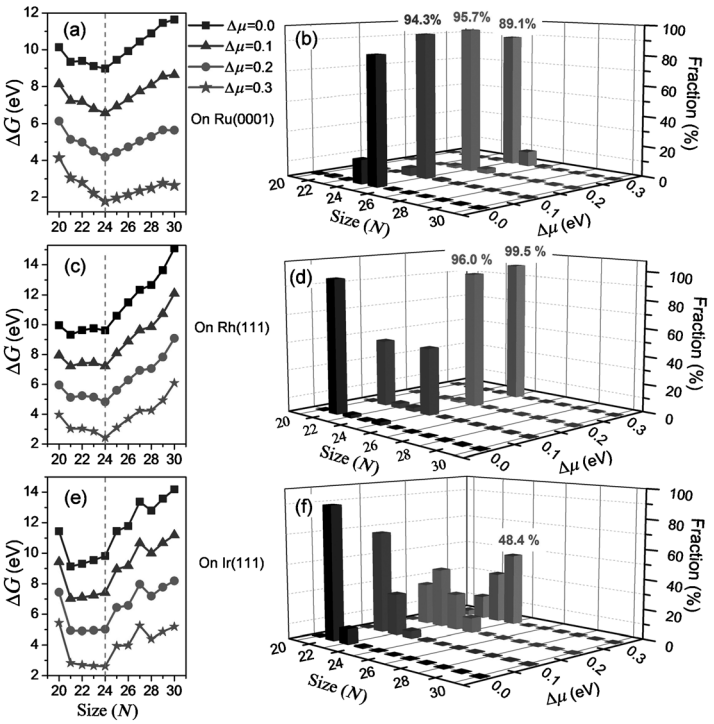

Figure 4. The Gibbs free-energies and populations of C_N ($20 \le N \le 30$) clusters under different condition of graphene growth (denoted by the chemical potential difference between feedstock and graphene, $\Delta\mu = 0.0$, 0.1, 0.2, and 0.3 eV) on a,b) Ru(0001). c,d) Rh(111), and e,f) Ir(111) surfaces, respectively.

In summary, using DFT calculations, we systemically investigated the stability of C_N clusters ($20 \le N \le 30$) on Ru(0001), Rh(111), and Ir(111) surfaces. Our study revealed a new type of ultrastable carbon clusters—branched sp^2 carbon networks. The most stable one of them, C_{21}-3C, was predicated to be the experimentally observed magic cluster in graphene CVD growth on both Ru(001) and Rh(111) surfaces by stability and population analyses. We also successfully explained why the uniform magic cluster only can be seen on Ru(0001) and Rh(111) surfaces but not on Ir(111) surface. This study provided a deep insight into the nucleation of graphene in the CVD growth processes and the formation mechanism of magic sized clusters might be used for the synthesis of graphene quantum dots.

Received: June 25, 2014
Published online: October 15, 2014

Keywords: supported carbon clusters · chemical vapor deposition · density functional calculations · graphene · derivative of sumanene

[1] D. Wei, Y. Lu, C. Han, T. Niu, W. Chen, A. T. S. Wee, *Angew. Chem. Int. Ed.* **2013**, *52*, 14121 – 14126; *Angew. Chem.* **2013**, *125*, 14371 – 14376.
[2] Q. Yuan, H. Hu, J. Gao, F. Ding, Z. Liu, B. I. Yakobson, *J. Am. Chem. Soc.* **2011**, *133*, 16072 – 16079.

[3] H. Wang, K. Sun, F. Tao, D. J. Stacchiola, Y. H. Hu, *Angew. Chem. Int. Ed.* **2013**, *52*, 9210 – 9214; *Angew. Chem.* **2013**, *125*, 9380 – 9384.
[4] C. N. R. Rao, A. K. Sood, K. S. Subrahmanyam, A. Govindaraj, *Angew. Chem. Int. Ed.* **2009**, *48*, 7752 – 7777; *Angew. Chem.* **2009**, *121*, 7890 – 7916.
[5] A. K. Geim, K. S. Novoselov, *Nat. Mater.* **2007**, *6*, 183 – 191.
[6] A. A. Balandin, S. Ghosh, W. Bao, I. Calizo, D. Teweldebrhan, F. Miao, C. N. Lau, *Nano Lett.* **2008**, *8*, 902 – 907.
[7] A. A. Balandin, *Nat. Mater.* **2011**, *10*, 569 – 581.
[8] C. Lee, X. Wei, J. W. Kysar, J. Hone, *Science* **2008**, *321*, 385.
[9] Y. Liu, B. Xie, Z. Zhang, Q. Zheng, Z. Xu, *J. Mech. Phys. Solids* **2012**, *60*, 591 – 605.
[10] X. Li, W. Cai, L. Colombo, R. S. Ruoff, *Nano Lett.* **2009**, *9*, 4268 – 4272.
[11] E. Loginova, N. C. Bartelt, P. J. Feibelman, K. F. McCarty, *New J. Phys.* **2009**, *11*, 063046.
[12] H. Chen, W. Zhu, Z. Zhang, *Phys. Rev. Lett.* **2010**, *104*, 186101.
[13] J. Gao, J. Yip, J. Zhao, B. I. Yakobson, F. Ding, *J. Am. Chem. Soc.* **2011**, *133*, 5009 – 5015.
[14] J. Gao, Q. Yuan, H. Hu, J. Zhao, F. Ding, *J. Phys. Chem. C* **2011**, *115*, 17695 – 17703.
[15] W. Zhang, P. Wu, Z. Li, J. Yang, *J. Phys. Chem. C* **2011**, *115*, 17782 – 17787.
[16] P. Wu, H. Jiang, W. Zhang, Z. Li, Z. Hou, J. Yang, *J. Am. Chem. Soc.* **2012**, *134*, 6045 – 6051.
[17] T. Niu, M. Zhou, J. Zhang, Y. Feng, W. Chen, *J. Am. Chem. Soc.* **2013**, *135*, 8409 – 8414.
[18] P. Wu, W. Zhang, Z. Li, J. Yang, *Small* **2014**, *10*, 2136 – 2150.
[19] B. Dai, L. Fu, Z. Zou, M. Wang, H. Xu, S. Wang, Z. Liu, *Nat. Commun.* **2011**, *2*, 522.
[20] X. Liu, L. Fu, N. Liu, T. Gao, Y. Zhang, L. Liao, Z. Liu, *J. Phys. Chem. C* **2011**, *115*, 11976 – 11982.
[21] J. D. Wood, S. W. Schmucker, A. S. Lyons, E. Pop, J. W. Lyding, *Nano Lett.* **2011**, *11*, 4547 – 4554.
[22] J. Gao, J. Zhao, F. Ding, *J. Am. Chem. Soc.* **2012**, *134*, 6204 – 6209.
[23] L. Gao, et al., *Nat. Commun.* **2012**, *3*, 699.
[24] Z. Li, W. Zhang, X. Fan, P. Wu, C. Zeng, Z. Li, X. Zhai, J. Yang, J. Hou, *J. Phys. Chem. C* **2012**, *116*, 10557 – 10562.
[25] G.-H. Lee, et al., *Science* **2013**, *340*, 1073 – 1076.
[26] A. M. Lewis, B. Derby, I. A. Kinloch, *ACS Nano* **2013**, *7*, 3104 – 3117.
[27] X. Zhang, L. Wang, J. Xin, B. I. Yakobson, F. Ding, *J. Am. Chem. Soc.* **2014**, *136*, 3040 – 3047.
[28] T. Ma, W. Ren, X. Zhang, Z. Liu, Y. Gao, L.-C. Yin, X.-L. Ma, F. Ding, H.-M. Cheng, *Proc. Natl. Acad. Sci. USA* **2013**, *110*, 20386 – 20391.
[29] H. Zhang, Q. Fu, Y. Cui, D. Tan, X. J. Bao, *J. Phys. Chem. C* **2009**, 113, 8296 – 8301.
[30] B. Wang, M. Caffio, C. Bromley, H. Früchtl, R. Schaub, *ACS Nano* **2010**, *4*, 5773 – 5782.
[31] Y. Zhang, L. Gomez, F. N. Ishikawa, A. Madaria, K. Ryu, C. Wang, A. Badmaev, C. Zhou, *J. Phys. Chem. Lett.* **2010**, *1*, 3101 – 3107.
[32] S. Nie, N. C. Bartelt, J. M. Wofford, O. D. Dubon, K. F. McCarty, K. Thürmer, *Phys. Rev. B* **2012**, *85*, 205406.
[33] Y. Cui, Q. Fu, H. Zhang, X. Bao, *Chem. Commun.* **2011**, *47*, 1470 – 1472.
[34] B. Wang, X. Ma, M. Caffio, R. Schaub, W.-X. Li, *Nano Lett.* **2011**, *11*, 424 – 430.
[35] J. Lu, P. S. E. Yeo, C. K. Gan, P. Wu, K. P. Loh, *Nat. Nanotechnol.* **2011**, *6*, 247 – 252.
[36] Q. Yuan, J. Gao, H. Shu, J. Zhao, X. Chen, F. Ding, *J. Am. Chem. Soc.* **2012**, *134*, 2970 – 2975.
[37] L. T. Scott, M. M. Hashemi, D. T. Meyer, H. B. Warren, *J. Am. Chem. Soc.* **1991**, *113*, 7082.
[38] H. Sakurai, T. Daiko, T. Hirao, *Science* **2003**, *301*, 1878.
[39] G. N. Sastry, E. D. Jemmis, G. Mehta, S. R. Shah, *J. Chem. Soc. Perkin Trans. 2* **1993**, 1867.
[40] U. D. Priyakumar, G. N. Sastry, *J. Phys. Chem. A* **2001**, *105*, 4488.
[41] T. Amaya, S. Seki, T. Moriuchi, K. Nakamoto, T. Nakata, H. Sakane, A. Saeki, S. Tagawa, T. Hirao, *J. Am. Chem. Soc.* **2009**, *131*, 408.
[42] T. Amaya, T. Hirao, *Chem. Commun.* **2011**, *47*, 10524.
[43] S. Armaković, S. J. Armaković, J. P. Šetrajčić, *Int. J. Hydrogen Energy* **2013**, *38*, 12190.
[44] H. Sakurai, T. Daiko, H. Sakane, T. Amaya, T. Hirao, *J. Am. Chem. Soc.* **2005**, *127*, 11580.
[45] T. Amaya, K. Mori, H.-L. Wu, S. Ishida, J. Nakamura, K. Murata, T. Hirao, *Chem. Commun.* **2007**, 1902.
[46] I. V. Markov, *Crystal Growth for Beginners: Fundamentals of Nucleation, Crystal Growth and Epitaxy*, 2ednd edWorld Scientific Publishing, Singapore, **2003**.
[47] J. Coraux, et al., *New J. Phys.* **2009**, *11*, 023006.

